Large convection cells as the source of Betelgeuse's extended atmosphere

Jeremy Lim*, Chris L. Carilli†, Stephen M. White‡, Anthony J. Beasley† & Ralph G. Marson†

** Academia Sinica Institute of Astronomy & Astrophysics, PO Box 1-87, Nankang, Taipei 115, Taiwan*

† National Radio Astronomical Observatory, Socorro, New Mexico 87801, USA

‡ Department of Astronomy, University of Maryland, College Park, Maryland 20742, USA

Supergiant stars such as Betelgeuse have very extended atmospheres, the properties of which are poorly understood. Alfvén waves[1–4], acoustic waves[1,2,5–7] and radial pulsations[8] have all been suggested as likely mechanisms for elevating these atmospheres and driving the massive outflows of gas seen in these stars: such mechanisms would heat the atmosphere from below, and there are indeed observations showing that Betelgeuse's extended atmosphere is hotter than the underlying photosphere[9,10]. Here we report radio observations of Betelgeuse that reveal the temperature structure of the extended atmosphere from two to seven times the photospheric radius. Close to the star, we find that the atmosphere has an irregular structure, and a temperature (3,450 ± 850 K) consistent with the photospheric temperature but much lower than that of gas in the same region probed by optical and ultraviolet observations[10]. This cooler gas decreases steadily in temperature with radius, reaching 1,370 ± 330 K by seven stellar radii. The cool gas coexists with the hot chromospheric gas, but must be much more abundant as it dominates the radio emission. Our results suggest that a few inhomogeneously distributed large convective cells (which are widely believed[11–16] to be present in such stars) are responsible for lifting the cooler photospheric gas into the atmosphere; radiation pressure on dust grains that condense from this gas may then drive Betelgeuse's outflow.

We observed Betelgeuse for 11 hours on 21 December 1996 with the Very Large Array (VLA) in its highest-resolution (A) configuration. At a wavelength of 7 mm, the angular resolution achieved is sufficient to have resolved Betelgeuse's optical disk, which subtends the largest angular diameter of any star visible in the night sky from the Northern Hemisphere. Because Betelgeuse's radio emission is purely thermal and optically thick (as demonstrated below), such spatially resolved radio observations also act as a pure thermometer of the stellar atmosphere. This is in contrast to observations in the ultraviolet continuum or optical and ultraviolet spectral lines, where the gas temperature is derived by comparison with theoretical model atmospheres. The VLA is at present equipped with 7-mm receivers on 13 of its 27 antennas. We used the remaining 14 antennas to observe at the longer wavelengths of 1.3, 2, 3.6 and 6 cm, where we found Betelgeuse to be partially resolved. Figure 1 shows the final image obtained at 7 mm. Betelgeuse's atmosphere becomes opaque at very different heights when observed at different wavelengths, and at 7 mm the average diameter is approximately twice that measured in the optical. The radio surface is clearly not spherically symmetric, nor does it appear to be axially symmetric.

To quantify the total flux and area of the 7-mm surface and hence its brightness temperature, we fitted circular and elliptical disks to the measured visibilities. The best fit was provided by a uniformly bright ellipse with dimensions of 95 ± 2 mas × 80 ± 2 mas at a position angle of 67° ± 7° (measured east from north), and a total flux density of 28.0 ± 5.6 mJy; the uncertainty in the flux measurements is dominated by the uncertainty in the absolute flux calibration of the VLA at 7 mm, estimated to be ±20%. Although this model ellipse does not provide a perfect fit to the observed disk structure, the residuals are small and approximately cancel in flux indicating that the total flux and area of the fitted ellipse nevertheless closely match that of the observed stellar radio disk. The implied brightness temperature is 3,450 ± 850 K (the uncertainty here, dominated by the uncertainty in the absolute flux calibration, represents extreme limits; elsewhere the quoted uncertainty refers to $\pm 1\sigma$), consistent with the stellar phospheric temperature of ~3,600 K (ref. 17). At the longer radio wavelengths—where Betelgeuse's atmosphere appears increasingly large while our angular resolution becomes progressively poorer—we derived just the average diameter and total flux density of the stellar radio disk by fitting uniformly bright circular disks to the measured visibilities at each wavelength. The increase in size with radio wavelength implies that the observed radio surfaces are optically thick, and hence have brightness temperatures reflecting the local gas temperature. In Fig. 2 we plot the measured brightness temperature of Betelgeuse's atmosphere as a function of stellar radius. The temperature of the atmosphere can be seen to decrease steadily with increasing radius from 3,450 ± 850 K at ~$2R_*$ to 1,370 ± 330 K at ~$7R_*$ (here R_* is the radius of the photosphere).

Our results are at odds with current theoretical and empirical models for the structure and temperature of Betelgeuse's atmosphere. Theoretical models which invoke the dissipation of Alfvén waves[1–4], shocks produced by acoustic waves[1,2,5–7], or shocks produced by

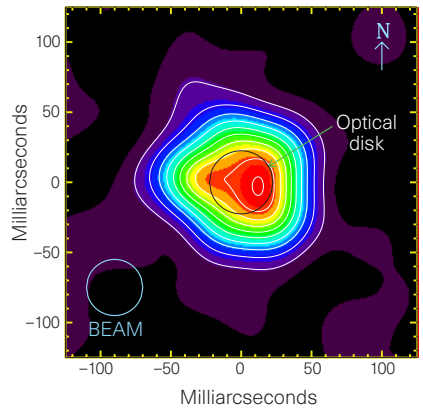

Figure 1 An image of Betelgeuse's atmosphere observed at a wavelength of 7 mm with the VLA. The angular resolution of this observation is 40 mas (blue circle at bottom left corner). White contour lines are plotted at 10%, 20%, …,90%, and 99% of the peak flux of the false-colour radio image. Betelgeuse's 7-mm surface has an average diameter approximately twice as large as its optical surface of diameter 45 mas (black circle with its centre placed coincident with the intensity-weighted centre of the radio disk), and is clearly not spherically symmetric. To make this image, we removed fast tropospheric phase fluctuations using a newly implemented "fast-switching" observing mode[24] at the VLA which allowed us to observe a nearby calibrator frequently without losing too much observing time. We therefore switched between Betelgeuse and an unresolved extragalactic object, 05528 + 03135 (used as our calibrator), located 4.2° away, with a cycle time of only ~2.5 min. To check the effectiveness of the amplitude and phase corrections, we also switched between 05528 + 03135 and another unresolved extragalactic object, 05326 + 07327 (used as our control source), located 5.3° away, at two intervals during the observation with the same cycle time; this yielded an unresolved image for the control source. We set the flux density scale using the primary flux calibrator 3C286. The final image includes a single iteration in phase self-calibration to correct for small residual phase errors: this self-calibrated image has a ~60% lower noise fluctuation level than the original image (consistent with the overall system noise), but is morphologically identical. Also, the final image was constructed using natural weighting of the visibilities but restored with a synthesized beam of size corresponding to that obtained using uniform weighting. The uniform weighted image is identical except for a slightly (35%) higher noise level, demonstrating the robustness of our conservative implementation of the super-resolution technique.

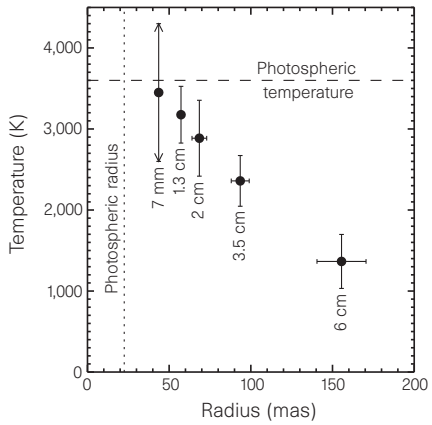

Figure 2 The temperature profile of Betelgeuse's atmosphere measured at the radio wavelengths indicated below each point. All the points have $\pm 1\sigma$ error bars, except for the 7-mm data point where the error bar with arrows indicate extreme limits (see text). The photospheric radius of 22.5 mas (ref. 17) is indicated by a dotted line, and the photospheric temperature of 3,600 K (ref. 17) is indicated by a dashed line. The stellar radius at 7 mm corresponds to the average radius measured in the spatially resolved image of Fig. 1. At the longer radio wavelengths, we derived the stellar radius by fitting a uniformly bright circular disk to the measured visibilities at each wavelength. The brightness temperature at each wavelength was calculated using the equation $T_b = 2.0 S_{mJy}(\lambda_{cm})^2/(\theta_{maj}\theta_{min})$ K, where S_{mJy} is the total flux density, λ_{cm} is the observing wavelength, and θ_{maj} and θ_{min} are the major and minor axes of the stellar radio disk, respectively, in arcseconds. We note that the derived brightness temperature is independent of any assumptions such as the distance to the star.

radial pulsations[8] to elevate the stellar atmosphere all predict a globally spherically symmetric structure, contrary to that in fact observed. Empirical models constructed to fit previous ultraviolet and radio data predict a spatially extended hot chromosphere[18,19], consistent with the idea that strong heating at low heights elevates the stellar atmosphere. The ultraviolet image of Betelgeuse taken with the Hubble Space Telescope (HST) clearly shows its chromosphere to have a diameter of 125 ± 6 mas in the continuum at 2,550 Å, which is inferred to be formed at a temperature of ~5,000 K (ref. 10). Our radio measurements, however, show that the hot chromospheric gas is not the only component at this height in Betelgeuse's atmosphere. The 2,550 Å height is above that which we probed at 7 mm, but is almost identical to that probed at 1.3 cm (diameter of 114 ± 4 mas). The temperature measured at 1.3 cm, however, is only 3,180 ± 350 K, formally below the photospheric temperature. From scans of the ultraviolet disk with the HST, the chromosphere observed in the Mg II h and k emission lines is inferred to extend to an even larger diameter of at least 270 mas (ref. 9). This surface is roughly comparable in diameter to that which we and others[19] have probed at 6 cm (diameter of 310 ± 30 mas), but here the temperature measured in radio is just 1,370 ± 330 K. An earlier speckle image of Betelgeuse's chromosphere observed in the Hα absorption line, which should be formed at a slightly higher temperature than the 2,550 Å continuum, showed a diameter of ~95 mas (ref. 20). This is comparable in diameter to our 7-mm measurement, but again the temperature measured in radio is much lower than is required for Hα absorption. Clearly, there are significant differences over the same height range between the temperature of the atmosphere inferred from optical and ultraviolet observations and the temperature directly measured in our radio observations.

We therefore conclude that the relatively cool gas responsible for the observed stellar radio emission spans the same height range as the hotter gas responsible for the optical and ultraviolet chromospheric signatures. To determine the conditions under which the cooler gas component could dominate the observed radio emission, we refer to the recent work by Reid and Menten[21] who studied the radio opacity of late-type giant star atmospheres. They showed that the radio opacity of gas at a temperature significantly below 4,000 K is provided by the interactions of electrons, obtained predominantly from elements with low ionization potentials such as potassium and sodium, with neutral atomic and molecular hydrogen. At temperatures above 4,000 K, corresponding to that of the hot chromospheric gas, scattering of electrons by protons (that is, ionized hydrogen atoms) provides the dominant source of radio opacity. As the electron–neutral absorption per neutral particle is a factor of about 10^3 smaller than the electron–ion free–free absorption per ion, the preferential detection of the cooler gas component in our radio observations implies that it must be more than 3 orders of magnitude more abundant than the chromospheric gas. Under these circumstances, it seems unlikely that the diffuse chromospheric gas plays an important role in elevating Betelgeuse's atmosphere.

Instead, the irregular structure and predominantly low temperatures of Betelgeuse's atmosphere suggest the following alternative mechanisms for elevating its atmosphere and driving its mass outflow. Over 20 years ago, Schwarzschild[11] proposed that late-type giant and supergiant stars possess very large convection cells, a few of which may be present on the stellar surface at any one time. The existence of such large convection cells has since gained wide acceptance in order to explain the polarized optical light commonly seen from these stars (see ref. 12 and references therein), as well as photospheric bright spots seen on the few red supergiants imaged[13–16], most notably Betelgeuse. Optical images of Betelgeuse show that the morphology of its photosphere changes with time, but at any given time can be well fitted by the superposition of one or more bright spots (which are not always required) on a circular stellar disk[13–16]. The HST ultraviolet image of Betelgeuse's atmosphere also appears to show a bright spot superposed on a circular disk[10]. Such large convection cells could elevate photospheric material into the stellar atmosphere[11,16] and, if distributed inhomogeneously over the stellar surface, produce an asymmetric atmospheric structure.

The elevation of photospheric material into the stellar atmosphere naturally explains our measurements of photospheric-like temperatures at small stellar radii, while the smooth decrease in temperature with increasing radius may represent expansion and cooling of the elevated material. Radiation pressure on dust grains condensed from the dense cool gas could then drive Betelgeuse's massive outflow. This mechanism has long been postulated for driving the massive cool outflows of late-type giant and supergiant stars[22], but faces severe difficulties if an extended inner region of the stellar atmosphere is entirely heated to chromospheric temperatures. Dust grains would then be required to form at relatively large stellar radii, where the gas density may in fact be too low for dust to condense effectively, or where radiation pressure may not be sufficiently intense to drive a massive outflow even if dust formation is possible. These problems are alleviated on Betelgeuse by the presence of dense cool gas in its inner atmosphere; indeed, dust has been detected to form episodically at radii as small as $\sim 4R_*$ (ref. 23). We note that the vigorous expulsion of gas into Betelgeuse's atmosphere would be expected to produce shock waves[16], which could heat localized but spatially distributed (and therefore extended) regions of its atmosphere to chromospheric temperatures. □

Received 21 November 1997; accepted 22 January 1998.

1. Hartmann, L. & MacGregor, K. B. Momentum and energy deposition in late-type stellar atmosphere and winds. *Astrophys. J.* **242,** 260–282 (1980).
2. Hartmann, L. & MacGregor, K. B. Wave-driven winds from cool stars. I. Some effects of magnetic field geometry. *Astrophys. J.* **247,** 264–268 (1982).
3. Holzer, T. E., Flå, T. & Leer, E. Alfvén waves in stellar winds. *Astrophys. J.* **275,** 808–835 (1983).
4. Hartmann, L. & Avrett, E. H. On the extended chromosphere of α Orionis. *Astrophys. J.* **284,** 238–249 (1984).
5. Ulmschneider, P. The chromospheric emission from acoustically heated stellar atmospheres. *Astron. Astrophys.* **222,** 171–178 (1989).

6. Cuntz, M. Chromospheric extents predicted by time-dependent acoustic wave models. *Astrophys. J.* **349,** 141–149 (1990).
7. Cuntz, M. On the generation of mass loss in cool giant stars due to propagating shock waves. *Astrophys. J.* **353,** 255–264 (1990).
8. Bowen, G. H. Dynamical modelling of long-period variable star atmospheres. *Astrophys. J.* **329,** 299–317 (1988).
9. Gilliland, R. & Dupress, A. K. *Stellar Surface Structure* (eds Strassmeier, K. G. & Linsky, J. L.) 165–172 (IAU Symp. No. 176, Kluwer, Dordrecht, 1996).
10. Gilliland, R. & Dupree, A. K. First image of the surface of a star with the Hubble Space Telescope. *Astrophys. J.* **436,** L29–L32 (1996).
11. Schwarzschild, M. On the scale of photospheric convection in red giants and supergiants. *Astrophys. J.* **195,** 137–144 (1991).
12. Doherty, L. R. On the polarization of Alpha Orionis. *Astrophys. J.* **307,** 261–268 (1986).
13. Buscher, D. F., Haniff, C. A., Baldwin, J. E. & Warner, P. J. Detection of a bright feature on the surface of Betelgeuse. *Mon. Not. R. Astron. Soc.* **245,** 7P–11P (1990).
14. Wilson, R. W., Baldwin, J. E., Buscher, D. F. & Warner, P. J. High-resolution imaging of Betelgeuse and Mira. *Mon. Not. R. Astron. Soc.* **257,** 369–376 (1992).
15. Klückers, V. A., Edmunds, M. G., Morris, R. H. & Wooder, N. Reality and the speckle imaging of stellar surfaces—II. The asymmetry of Alpha Orionis. *Mon. Not. R. Astron. Soc.* **284,** 711–716 (1997).
16. Tuthill, P. G., Haniff, C. A. & Baldwin, J. E. Hotspots on late-type supergiants. *Mon. Not. R. Astron. Soc.* **285,** 529–539 (1997).
17. Dyck, H. M., Benson, J. A., van Belle, G. T. & Ridgway, S. T. Radii and effective temperatures of K and M giants and supergiants. *Astron. J.* **111,** 1705–1712 (1996).
18. Skinner, C. J. & Whitmore, B. The circumstellar environment of α Orionis. *Mon. Not. R. Astron. Soc.* **224,** 335–348 (1987).
19. Skinner, C. J. *et al.* Circumstellar environments—V. The asymmetric chromosphere and dust shell of α Orionis. *Mon. Not. R. Astron. Soc.* **288,** 295–306 (1997).
20. Hebden, J. C., Eckart, A. & Hege, E. K. The Hα chromosphere of Alpha Orionis. *Astrophys. J.* **314,** 690–698 (1987).
21. Reid, M. J. & Menten, K. M. Radio photospheres of long-period variable stars. *Astrophys. J.* **476,** 327–346 (1997).
22. Kwok, S. Radiation pressure on grains as a mechanism for mass loss in red giants. *Astrophys. J.* **198,** 583–591 (1975).
23. Bester, M. *et al.* Measurement at 11 micron wavelength of the diameters of α Orionis and α Scorpii, and changes in effective temperature of α Orionis and very recent dust emission. *Astrophys. J.* **463,** 336–343 (1996).
24. Carilli, C. L., Holdaway, M. A. & Sowinski, K. P. *Fast Switching at the VLA* (VLA Scientific Memo. no. 169, National Radio Astronomical Observatory, Socorro, NM, 1996).

Acknowledgements. The VLA is a facility of the National Radio Astronomy Observatory, which is operated by Associated Universities, Inc., under cooperative agreement with the National Science Foundation. We thank B. Butler for providing us with the ellipse-fitting algorithm.

Correspondence and requests for materials should be addressed to J.L. (e-mail: jlim@biaa.sinica.edu.tw).

Extreme oxygen-isotope compositions in magnetite from unequilibrated ordinary chondrites

Byeon-Gak Choi*†‡, Kevin D. McKeegan*, Alexander N. Krot†§ & John T. Wasson*†

** Department of Earth and Space Sciences, †Institute of Geophysics and Planetary Physics, University of California, Los Angeles, California 90095-1567, USA*

§ Hawai'i Institute of Geophysics and Planetology, School of Ocean and Earth Science and Technology, University of Hawai'i, Honolulu, Hawaii 96822, USA

Primitive meteorites (such as the unequilibrated ordinary chondrites) have undergone only minor thermal processing on their parent asteroids, and thus provide relatively unaltered isotopic records from the early Solar System. For terrestrial materials, oxygen isotope compositions form a linear array called the terrestrial fractionation line[1]. In meteorites the oxygen isotopic composition commonly deviates from this line[2], the magnitude of the deviation being expressed by the quantity $\Delta^{17}O$. Such deviations, which cannot be explained by mass-dependent fractionation processes, are probably caused by the mixing of two or more nebular components having different nucleosynthetic histories, for example, solids and gas. But no direct evidence for the oxygen isotopic composition of the latter (which is the dominant oxygen reservoir) has hitherto been available. Here we report *in situ* oxygen-isotope measurements of magnetite grains in unequilibrated ordinary chondrites. Magnetite (which formed by aqueous alteration of metal in the parent asteroid) may serve as a proxy for nebular H_2O. We measured a value of $\Delta^{17}O \approx 5‰$, much higher than typical values of 0–2‰ in ordinary-chondrite silicate grains. Our results imply that a nebular component of high-$\Delta^{17}O$ H_2O was incorporated into the parent asteroid of the unequilibrated ordinary chondrites.

The discovery of large oxygen-isotope variations both within[3] and among[4] the chondrite groups demonstrated the existence of significant isotopic heterogeneities in the solar nebula. At the places and times in the nebula where the chondrite groups (or sets of related groups) formed, nebular grains incorporated material from reservoirs having distinct oxygen-isotope compositions reflecting different nucleosynthetic histories. An important factor is the unique cosmochemistry of oxygen that simultaneously makes it the dominant rock-forming element as well as one of the principal components of the nebular gas phase. For this reason, disequilibrium oxygen-isotope distributions among meteorites are commonly modelled in terms of two reservoirs, one solid, the other gaseous (see, for example, Clayton and Mayeda[5]).

In minerals from unequilibrated ordinary chondrites (UOCs), major cations such as Mg^{2+} and Fe^{2+} have not exchanged appreciably since formation in the nebula, and in most silicates, O diffuses more slowly than these ions[6,7]. Thus most minerals retain their nebula compositions. However, fluid transported along grain surfaces in asteroids has produced some new, low-temperature minerals, for example magnetite[8] and phyllosilicates[9].

A minor subset of UOCs contain magnetite (Fe_3O_4)-carbide assemblages; Krot *et al.*[8] inferred that the magnetite resulted from oxidation of Fe–Ni metal, probably by H_2O in an asteroid. Because all the oxygen in magnetite comes from the oxidant, the study of magnetite can constrain the O-isotope composition of the oxidizing fluid.

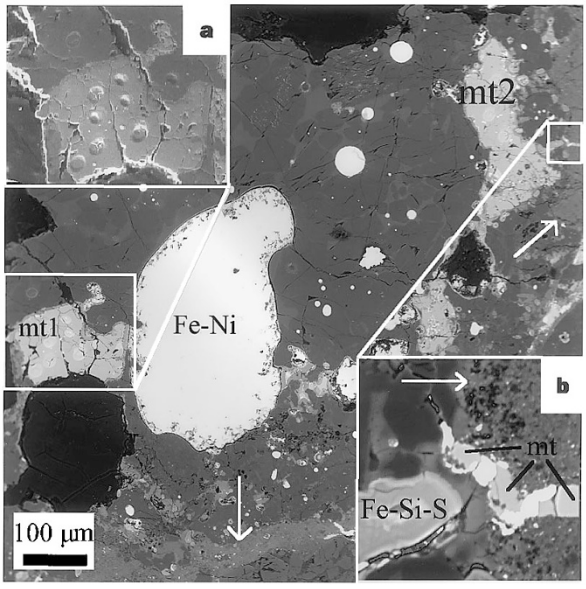

Figure 1 Back-scattered-electron image of part of low-FeO porphyritic olivine chondrule (PO1) in Semarkona USNM1805-5. Arrows indicate boundaries between the chondrule and matrix. In the chondrule white nodules are Fe–Ni metal with taenite, carbides and troilite. Light-grey objects with irregular shapes are magnetite (mt1 and mt2); the magnetite grains are surrounded by fayalite-like minerals ~5 μm thick. Dark areas on top of the image and at bottom of mt1 are plucked regions. **a**, Scanning electron microscopy image of mt1, showing seven craters formed by ion-microprobe sputtering. **b**, High-magnification back-scattered-electron image of chondrule–matrix boundary. A magnetite-bearing vein extends from the chondrule into the matrix implying that this vein formed after the chondrule and matrix were compacted together.

‡ Present address: Division of Geological and Planetary Sciences, California Institute of Technology, Pasadena, California 91125, USA.